Cobalt nanoclusters on metal-supported Xe monolayers: Influence of the substrate on cluster formation kinetics and magnetism

V. Sessi,* K. Kuhnke, J. Zhang,† J. Honolka,‡ and K. Kern
Max-Planck-Institut für Festkörperforschung, Heisenbergstrasse 1, 70569 Stuttgart, Germany

A. Enders
Department of Physics and Astronomy and MCMN, University of Nebraska, Lincoln, Nebraska 68588, USA

P. Bencok§
European Synchrotron Radiation Facility, 6 rue Jules Horowitz, BP 220, 38043 Grenoble Cedex 9, France

S. Bornemann, J. Minár, and H. Ebert
Department Chemie und Biochemie, Ludwig-Maximilians-Universität München, 81377 München, Germany
(Received 5 September 2009; revised manuscript received 1 April 2010; published 4 May 2010)

The growth dynamics of submonolayer coverages of cobalt during buffer-layer assisted growth on Ag(111) and Pt(111) substrates is investigated by variable temperature scanning tunneling microscopy in the temperature range between 80 and 150 K. It is found that attractive cluster-substrate interactions can govern the cluster formation on the Xe buffer layer if the Xe layer is sufficiently thin. The interpretation of the microscopy results is supported by x-ray magnetic circular dichroism data which monitor the effect of cluster-substrate interactions on the formation of magnetic moments and magnetic anisotropy of Co nanocluster during the different stages of growth. *Ab initio* calculations show that the cluster magnetism is controlled by the interface anisotropy, leading to perpendicular magnetization for Co on Pt(111). Limits of and new potential for nanocluster fabrication by buffer-layer-assisted growth are discussed.

DOI: 10.1103/PhysRevB.81.195403 PACS number(s): 61.46.Bc, 68.37.Ef, 75.75.−c, 75.30.Gw

I. INTRODUCTION

A fundamental physical understanding of magnetic nanostructures in contact with a medium is essential from a technological point of view: the magnetocrystalline anisotropy energy (MAE) and the superparamagnetic blocking temperature T_B come to depend not only on the nanostructure material itself but also on the electronic and magnetic properties of the supporting medium and, in particular, on the contact area between the two. Thus, there is a critical need for versatile synthesis strategies that permit the fabrication of nanoclusters at surfaces with well-defined magnetic functionality and with unprecedented control over the cluster size, shape, size distribution, areal density, and even positional accuracy.

The synthesis of nanoclusters by buffer-layer assisted growth (BLAG) (Ref. 1) has become an increasingly attractive strategy to form clusters at surfaces, both for its simplicity and for its potential to be a generic approach to fabricate clusters of any material, also ordered cluster arrays, on all kinds of surfaces. Here, a noble-gas layer acts as a buffer between the substrate and deposited single atoms which self-assemble on the layer and form nanostructures. The role of the noble-gas layer is to decouple the cluster material from the substrate so that the cluster formation is unimpeded by the substrate. It has been reported in several publications that the final cluster size and the areal distribution only depend on the thickness of the Xe buffer layer and the metal coverage, thus offering a desirable way to grow "anything on anything."[2,3]

Recent experimental and theoretical work has shown, however, that also BLAG is crucially dependent on many experimental parameters and that it is not a "one size fits all" method to produce clusters. For instance, it has been shown that in some cases the van der Waals interactions between the clusters and the substrate can effectively pull the clusters into the Xe layer.[4] It was also claimed that at least 60 monolayers (MLs) of buffer layer is necessary to electronically decouple the metal clusters from the substrate.[5] Finally, wetting of the nanoclusters by xenon and therefore partial embedding into the xenon layer has been predicted by molecular-dynamics simulations.[6] These results indicate that the cluster formation is the result of a rather complex interplay between the atoms from the substrate, the buffer layer, and the deposited atoms, yet to be understood.

Nanoscale effects on the Co growth due to interactions with the surrounding material are expected to be of paramount importance when the system is reduced to a submonolayer amount of metal on a very thin rare-gas layer. We have already demonstrated that indeed, under these conditions, the morphology of the substrate underneath can be used as a template to tailor the cluster size and their lateral arrangement on the substrate.[7,8]

In the present paper we investigate the mechanisms driving the dynamics during BLAG in detail, focusing on the early stage of cluster formation. The combined use of variable temperature scanning tunneling microscopy (VT-STM) and x-ray magnetic circular dichroism (XMCD) measurements allows us to monitor directly the growth mechanism of Co/Xe in case of absorption on two electronically very different metal substrates: Ag(111) and Pt(111). This work shows how the interface properties determine not only the morphology but also the magnetic properties of the cluster

system. The measured magnetic moments and magnetic anisotropy are compared to *ab initio* magnetic calculations of monolayer, bilayer and trilayer Co epitaxial island systems of various size deposited on Ag(111) and on Pt(111). Among other things from this comparison it becomes evident that the MAE, that emerges upon contact with the surface, is a pure interface effect. For a detailed description of the sample preparation and the experimental parameters we refer the reader to Appendix.

II. CLUSTER GROWTH ON THICK XENON BUFFER LAYERS

A. Cluster growth and morphology

The morphology of Co clusters formed with comparatively thick Xe layers on Ag(111) was studied with VT-STM. The Xe thickness was controlled by the exposure of the clean Ag(111) substrates to Xe partial pressures in UHV at substrate temperatures of 30 K. For determination of the Xe thickness we used an experimentally established estimate, 1 ML Xe=5.5 Langmuir (L), from Ref. 9 (1 L=1 sec 10^{-6} Torr). Thus, exposure of the substrate to 50 L resulted in Xe buffer layers of approximately 9 ML thickness. Cobalt was deposited on the Xe buffer layer at $T=30$ K by thermal evaporation from a Co rod. For the samples in this section 5% of a full epitaxial Co monolayer have been deposited. STM images were taken at different temperatures while warming up the sample to room temperature. In Fig. 1, STM topography images are displayed taken at temperatures of (a) 100 K, [(b) and (c)] 140 K, [(d) and (e)] 150 K, and (f) at 300 K, after full Xe desorption. The images show clearly the desorption of the Xe buffer layer, and the presence and ripening of Co clusters. In (a) small clusters of about 1–2 nm diameter can already be resolved on a rather noisy background. The overall quality of the images is reduced by the diminished electron tunneling through the noble gas as well as the weak bonds of the adlayer atoms to the substrate. However, it is clearly visible how the Xe layer breaks up into islands surrounding the Co clusters at about 140 K [Figs. 1(b) and 1(c)]. The boundary from a continuous to an interrupted Xe layer can best be seen at the bottom of Fig. 1(c). Several hours elapsed between the acquisition of images (b) and (e). From the images (a)–(e) we conclude that the desorption of Xe from Ag(111) occurs at temperatures above $T=100$ K and it is especially pronounced in the temperature window between 140 and 150 K. A delay of desorption of Xe is visible at defects such as substrate steps and Co clusters. The Xe is completely removed at substrate temperatures above 150 K.

The Xe desorption temperature in bulk is about 55 K. However, monolayer or bilayer systems of xenon on a metal surface are thermally more stable due to increased binding forces.[10] It is therefore reasonable to assume that the desorption of Xe is a two-step process. In a first step at the bulk desorption temperature, the entire Xe layer desorbs except of the first and second monolayer that are in direct contact with the metal substrate. In a second step the residual Xe is removed by warming up the sample to higher temperatures, which are determined by the intensity of the Xe-substrate

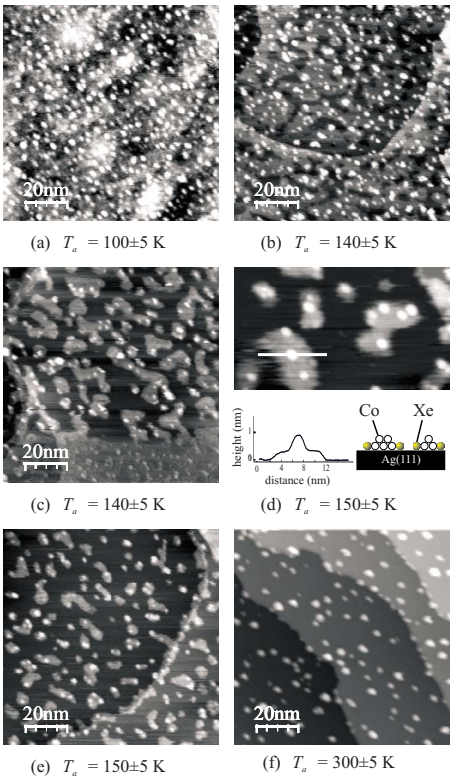

FIG. 1. (Color online) STM topographies for thick xenon buffer layers: Co/thick Xe layer/Ag(111) deposited at 30 K and then annealed to progressively higher temperatures T_a as indicated in the caption; (d) zoom-in of image (e) together with a line scan over a Co cluster and a cartoon showing the Co immersed in Xe.

interaction. In the specific case of Xe/Ag(111) the last Xe layer remains on the surface up to 85–90 K.[11] Thus, the observed desorption temperature of 150 K in presence of Co nanoclusters is significantly higher than both desorption temperatures of the bulk Xe and of the Xe ML on Ag(111).

In order to get information on the cluster size, a direct evaluation of volume by height profiles of single clusters in STM images is not adequate here, for two reasons. First, our images do not show atomic resolution or atomiclike features on the clusters and on the substrate, which complicates the estimate of the tip-convolution effects. Second, in some cases, for example, in Fig. 1(a), the border between a cluster and the Xe matrix is undefined. Thus, we preferred to determine the cluster size from the nominal Co coverage read by a Quartz Micro-Balance and from the cluster density in STM images. In this way, we have obtained an increasing average number of atoms per cluster with temperature of about 20 ± 5 atoms at 100 K, 40 ± 7 atoms at 140 K, and about 50 ± 5 atoms at room temperature. The given error here is the statistic error found after averaging over several images of the samples.

At room temperature a broad cluster size distribution is observed, as seen in Fig. 1(f). The given value of about 50 atoms per cluster is an average value: smaller clusters are visible in the vicinity of step edges and larger clusters are located on surface terraces. Step decoration is typically seen for clusters made by BLAG on weakly interacting surfaces, such as Ag and Cu, as shown in our previous work.[8]

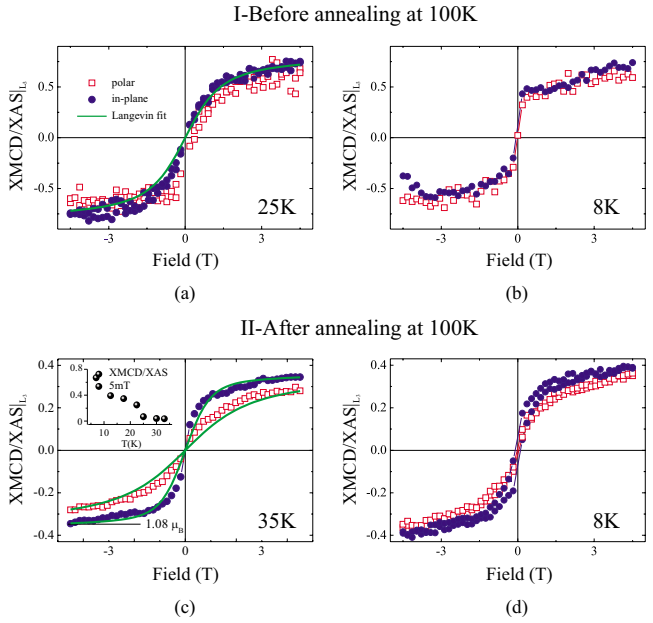

FIG. 2. (Color online) Magnetic characterization of 0.05 ML Co/thick Xe layer/Ag(111) [(a) and (b)] before and [(c) and (d)] after annealing at 100 K; [(a) and (b)] hysteresis curves at 25 and 8 K taken right after Co deposition on the Xe buffer layer; [(c) and (d)] hysteresis curves at 35 and 8 K taken after annealing the sample to 100 K with consequent desorption of the bulk Xe, cluster growth and contact with the substrate. The inset in (c) shows quasiremanence measurements at $B=5$ mT; the full lines in the hysteresis plot correspond to a Langevin fit according to Eq. 5 in Ref. 14. The magnetic moment used in the fits are (a) the Co bulk value and (b) the calculated values displayed in Table I. In the latter case, $n_h=2.49$ (Co bulk value) and μ_T is derived from the *ab initio* calculations (Table III). The slight asymmetry in the hysteresis curve in (b) is not a real effect but within the larger error margins for TEY experiments on the thick (semi-insulating) Xe layer.

B. Magnetism of Co clusters on Ag(111)

Magnetic properties such as spin and orbital moments, and, in particular, the magnetic anisotropy, are known to be highly sensitive to cluster size, geometry, and interface effects. The XMCD technique provides surface sensitive information on these magnetic parameters and therefore allows to extract information on the sample structure. We studied the magnetic properties of the cobalt clusters during classic BLAG with 12 ± 1 layers of xenon and a cobalt coverage of 0.05 ML. Details about the experimental procedure are given in the appendix in Sec. VII.

Figure 2 (top) shows hysteresis curves taken shortly after Co deposition at two different temperatures. The ordinate shows the ratio of the intensities of the XMCD and the x-ray absorption spectra (XAS) evaluated at the peak of the L_3 edge. To first approximation this ratio is proportional to the magnetization, XMCD/XAS $\propto M$, where M is the average magnetization of the sample. We find that none of the magnetization curves in (a) and (b) show remanent magnetization at zero field. In addition, the curves are isotropic, i.e., they do not show any difference between polar ($\phi=0°$) and in-plane ($\phi=70°$) magnetic field directions, where ϕ is the angle of the field with the substrate normal. Reasons for this apparent absence of magnetic anisotropy could be an amorphous cluster structure, a random distribution of the cluster easy axis or even a partial realignment of the clusters on the Xe layer in the presence of a torque created by the magnetic field. A fit to the in-plane magnetization curves with a standard Langevin function, which includes the magnetic moment of bulk Co taken from Ref. 12, yields a spin block size $N=35\pm5$ atoms.

TABLE I. Magnetic properties of 0.05 ML Co/thick Xe layer/Ag(111) before and after annealing at 100 K. The average magnetic moments per d-band holes given in units of μ_B have been calculated from the saturated XMCD data at $T=8$ K using the sum rules with the magnetic field in plane and polar with respect to the surface normal. The value of the XMCD/XAS ratio at the L_3 absorption edge is also indicated.

	$\frac{\mu_L}{n_h}$	$\frac{(\mu_S+7\mu_T)}{n_h}$	$\frac{\text{XMCD}}{\text{XAS}}$
I-Before annealing at 100 K			
In-plane (8 K)	–	–	0.74 ± 0.05
Polar (8 K)	–	–	0.64
II-After annealing at 100 K			
In-plane (8 K)	0.08 ± 0.04	0.46 ± 0.04	0.40
Polar (8 K)	0.07	0.33	0.36

The scenario changes upon desorption of the bulk xenon when the sample is annealed at 100 K. In Figs. 2(c) and 2(d) we show hysteresis curves taken after Xe desorption and cooling the sample back to 35 K and 8 K, respectively. While the cobalt moments show no sign of anisotropy on the Xe layer, anisotropy emerges when the clusters make contact with the surface. The in-plane direction now is an easy axis. For this system we were able to apply the sum rules for $3d$ metals[13] to find the Co orbital and effective spin moment μ_L and $\mu_S'=\mu_S+7\mu_T$. Here, μ_S is the spin moment and μ_T is the intra-atomic magnetic dipole moment that is usually calculated by *ab initio* theory. Magnetic moments per d-band hole (n_h) are summarized in Table I. Using bulk Co values $n_h=2.49$ and the theoretical values for μ_T (see Sec. IV), one can calculate the average total magnetic moment $\mu=\mu_L+\mu_S$. The latter is used to find the value of the MAE via a superparamagnetic fit using the procedure described in Ref. 14, assuming a substrate induced uniaxial symmetry in the magnetic anisotropy. We obtain a hard axis in the polar direction with a MAE of -0.15 ± 0.1 meV/atom and a spin block size of $N=52\pm5$ atoms. The latter value is slightly larger than the cluster size of about 20–40 atoms found in Sec. II A. However, there is still sufficient agreement, an indication that the thermodynamic model employed to describe the nanoclusters magnetization is reasonable for our system. Further, an upper estimate to the blocking temperature T_B of the clusters is obtained from temperature-dependent measurements of the magnetization at small applied fields of $B=5$ mT shown in the inset of Fig. 2(c). Here, for each temperature data point the magnetic field was ramped up to 4.5 T to saturate the magnetization and then down to 5 mT before measuring the dichroic signal. In this

way, the magnetization observed was due to the fraction of clusters that were still blocked at that temperature and that magnetic field. From the temperature at which the magnetization has dropped below $1/e$ of the maximum value after saturating the sample at lowest temperatures we find $T_B < 25 \pm 5$ K. The standard expression for T_B can also be used here,

$$T_B = \frac{N \cdot \mathrm{MAE}}{k_B \ln(\tau_m/\tau_0)}.$$

k_B is the Boltzmann constant, τ_m the experimental measurement time (300 s in our case), and τ_0 the relaxation time of the system (typically, between 10^{-9} and 10^{-10} s). For our system the above formula gives a value of $T_B = 4.5 \pm 2$ K, in agreement with the upper estimation and with observation of blocking at 8 K.

We want to point out that in the case of Co situated on thick Xe layers the signal-to-noise ratio in the XMCD was insufficient for a quantitative evaluation of the moments. Thus, in this case only the XMCD/XAS ratio at the L_3 absorption edge is shown in Table I.

III. BUFFER-LAYER ASSISTED GROWTH WITH ATOMICALLY THIN XENON LAYERS

A. Co cluster morphology on Ag(111) and Pt(111)

In order to address the question if atoms or clusters interact with the substrate long before the last monolayer of the noble gas is desorbed we studied the extreme case of BLAG with only a single layer (5 L) of xenon. As substrates we used Ag(111) and Pt(111). The Co coverage was again 5% of an epitaxial monolayer, in analogy to the samples in the previous section. Differently from the Xe on Ag(111) system, where the lattice constants of Xe and Ag are always incommensurate,[15,16] Xe grows on Pt(111) as a commensurate layer below coverages of $\Theta \simeq 0.33$ ML.[17] At higher coverages a transition from commensurate to incommensurate occurs.[17] The Xe desorption temperature for 1 ML Xe/Pt(111) is about 100–110 K, which is significantly higher than on Ag(111), due to a higher binding energy.[18]

STM images taken on 0.05 ML Co/1 ML Xe/Ag(111), as well as on 0.05 ML Co/1 ML Xe/Pt(111), in the temperature range between 80 and 300 K are summarized in Fig. 3. At low temperatures, when the complete Xe monolayer is still adsorbed and cluster formation is in its early stage, we can hardly distinguish the clusters from the Xe background [see Figs. 3(a) and 3(b)].

In the case of Ag(111) [Fig. 1(a)] one observes streaks in the STM which points to a displacement of mobile Co clusters or Xe atoms by field-induced diffusion while scanning the tip over the surface. Terrace step edges as well as defects and vacancies in the Xe layer provide an energetically favorable position where the Co clusters are more strongly bound and therefore immobile. A similar behavior as observed in the previous paragraph for thicker xenon films [Fig. 1(e)] is found instead upon annealing [Fig. 3(c)], that is residual Xe on the surface is pinned at Co clusters up to 150 K.

For the BLAG on Pt(111) the dynamics is different. We observe no streaks at lowest temperatures in Fig. 3(b) but an

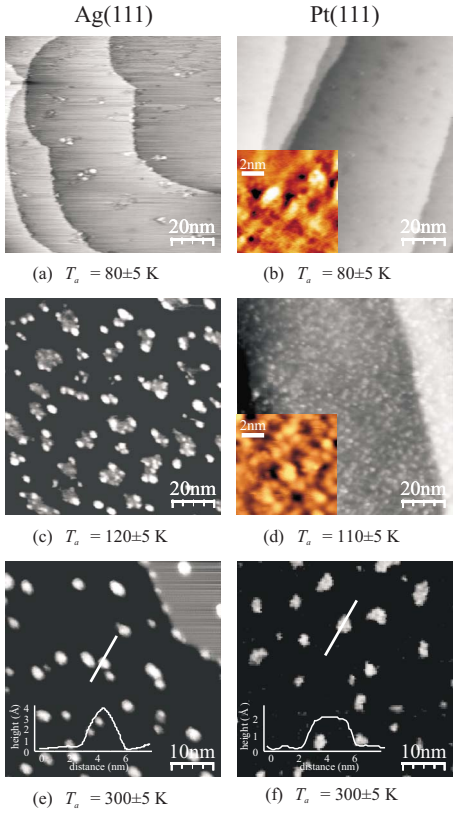

FIG. 3. (Color online) STM topographies for Co/thin Xe layer/Ag(111) (left column) and Co/thin Xe layer/Pt(111) (right column) taken after annealing at T_a indicated in the figure caption. The scanning temperature was 20 K for (a)–(d) and 300 K for (e) and (f). The inset in (e) and (f) shows the line scan across a Co island supported on the two different substrates.

increase in the apparent height corrugation Δh when warming the sample from 80 K ($\Delta h \approx 0.2$–0.4 Å) to 110 K [$\Delta h \approx 0.6$ Å, Fig. 3(d)] and finally to 150 K ($\Delta h \approx 1.6$ Å, not shown). Our conclusion from these and many other STM images is that the clusters are actually buried in the Xe buffer layer and become exposed as the Xe layer desorbs. Further increase in the temperature up to RT [Figs. 3(e) and 3(f)] produces in both cases an increase in the cluster size accompanied by a reduction in the density as observed in Fig. 1(f). For Ag(111) the clusters are of double layer height and the average cluster size estimated from the STM data is now $N = 16 \pm 5$ at 120 K and $N = 44 \pm 5$ at RT. On the Pt(111) surface we have islands of ML height with an average number of atoms that changes from $N = 6 \pm 4$ at 110 K to $N = 62 \pm 10$ at RT. We can conclude that using constant BLAG parameters the system-dependent growth dynamics can lead to structures with substantially different properties on the two substrates: small compact three-dimensional structures on the Ag(111) [Fig. 3(e)] and monolayer islands for the Pt(111) [Fig. 3(f)]. We infer from these experiments that in the case of a thin Xe layer the substrate does have considerable influence during buffer-layer assisted growth and contributes to the final size, shape, and distribution of the clusters.

TABLE II. Magnetic properties for the samples Co/thin Xe layer/Ag(111) and Co/thin Xe layer/Pt(111) before and after annealing at 100 K. The average magnetic moments per *d*-band holes given in units μ_B have been calculated from the saturated XMCD data at the indicated temperatures using the sum rules with the magnetic field in plane and polar with respect to the surface normal. The value of the XMCD/XAS ratio at the L_3 absorption edge is also indicated.

	$\frac{\mu_L}{n_h}$	$\frac{(\mu_S+7\mu_T)}{n_h}$	$\frac{\text{XMCD}}{\text{XAS}}$
I-Before annealing at 100 K			
Ag(111) in plane (25 K)	0.10 ± 0.04	0.53 ± 0.04	0.60 ± 0.05
Ag(111) polar (25 K)	0.11	0.60	0.65
Pt(111) in plane (25 K)	–	–	0.45
Pt(111) polar (25 K)	0.16	0.54	0.76
II-After annealing at 100 K			
Ag(111) in plane (8 K)	0.11	0.49	0.51
Ag(111) polar (8 K)	–	–	0.46
Pt(111) in plane (8 K)	–	–	0.38
Pt(111) polar (8 K)	0.12	0.57	0.61

B. Comparison of the magnetism of Co clusters on Ag(111) and Pt(111) substrates

The magnetism of the samples shown in Sec. III A has been investigated by XMCD. We have taken angular-dependent x-ray absorption spectra at the Co $L_{3,2}$ edges, as a function of temperature and magnetic field. The clusters considered in the following have been synthesized by BLAG using 0.05 ML Co and 3–4 ML Xe.

The complete set of magnetic moments deduced from the XMCD data are shown in Table II for the two samples made on the Ag(111) and Pt(111) substrates, before and after annealing at 100 K. The XMCD was measured at magnetic fields of $B=4.5$ T. The hysteresis curves obtained on those samples along the sample normal and under grazing incidence are summarized in Fig. 4, again before and after Xe desorption. At low temperatures for Co situated on xenon/Ag(111) the magnetization is isotropic [Fig. 4(a)], in analogy to what is observed in Figs. 2(a) and 2(b) for the case of thick buffer layers. On the other hand Co nanostructures on xenon/Pt(111) show a strikingly pronounced magnetic easy axis in the polar direction [Fig. 4(b)], which endorses our STM interpretation of a stronger tendency of cobalt to penetrate the xenon. After annealing both samples at $T=100$ K and measuring again at 25 and 8 K [Figs. 4(c)–4(f)] in both cases, Ag(111) and Pt(111), a magnetic anisotropy is visible in the magnetization curves: while Co/Pt(111) still has a strong polar easy axis, Co prefers the in-plane direction in the case of the Ag(111) substrate.

The MAE was estimated in the superparamagnetic regime from the Co magnetization curves on Pt(111) at 25 K (before and after annealing at 100 K), and on Ag(111) at 8 K, using

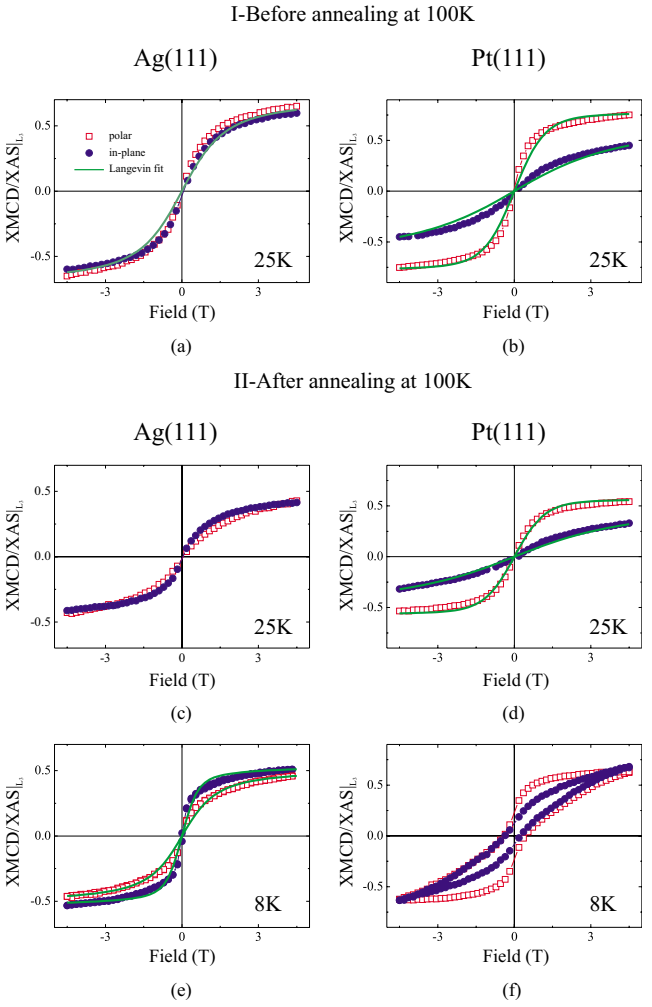

FIG. 4. (Color online) Magnetic characterization of the systems in Fig. 3: 0.05 ML Co/thin Xe layer/Ag(111) (left column) and 0.05 ML Co/thin Xe layer/Pt(111) (right column): [(a) and (b)] before and [(c)–(f)] after annealing at 100 K, measured at [(c) and (d)] 25 K and [(e) and (f)] 8 K. The full lines in the hysteresis plot correspond to a Langevin fit according to Eq. 5 in Ref. 14. The magnetic moment used in the fits are the calculated values displayed in Table II with $n_h=2.49$ (Co bulk value) and μ_T derived from the *ab initio* calculations (Table III).

the procedure described earlier. We obtain a magnetic anisotropy of +0.6 and +0.67 meV/atom for Co/Pt before and after annealing at 100 K, and −0.10 meV/atom for Co/Ag. An additional average induced moment per Co atom due to the platinum nearest-neighbor atoms was included in the calculation. In particular, for each Co atom one Pt magnetic moment of $\mu_{Pt}=0.15$ μ_B/atom (Ref. 19) was added, since one Co atom has three Pt neighbors, but each Pt atom is shared among three Co atoms. For the spin block size we then get $N=17\pm5$ and $N=18\pm5$ before and after annealing at 100 K for Pt(111) and $N=25\pm5$ and $N=18\pm5$ for Ag(111). Also in this case the agreement with the cluster size found by STM measurements above $T=80$ K (Sec. III A) is reasonable. Remanence is observed at lowest temperatures of 8 K in the case of the Pt(111) substrate due to the strong polar MAE which pushes the blocking temperature to higher values.

IV. *AB INITIO* CALCULATIONS OF MAGNETIC Co*N* ISLANDS ON Ag(111) AND Pt(111)

In order to interpret the experimentally observed trends in the magnetic properties of these deposited Co clusters we performed *ab initio* calculations within the local-density approximation of density-functional theory (DFT),[20] using the spin-polarized relativistic Korringa-Kohn-Rostoker multiple-scattering formalism.[21] In this scheme, the Dirac Green's function was calculated self-consistently for large single and multilayer Co islands assuming pseudomorphic deposition on a 38-layer Ag (Pt) slab having the experimental lattice constant of 4.085 (3.924) Å. Furthermore we applied the atomic sphere approximation to the potentials and neglected lattice relaxations (see Refs. 14 and 19 for more details). In order to obtain converged results for the magnetic anisotropy energies we used here a logarithmic mesh for the energy contour integration as described in Ref. 22. This leads to slight changes in the orbital magnetic moments when compared to the results of Co_N/Pt(111) in Ref. 19 where a different energy mesh was used.

The influence of coordination effects on the magnetism of the deposited Co clusters was studied by a systematic increase in the island size. Table III shows calculated spin (μ_S), orbital (μ_L), and intra-atomic dipolar moment (μ_T) and MAE. For the system Co/Pt(111) we find an out-of-plane easy-axis direction at every island size with the exception of Co3 and Co7 where the anisotropy is slightly in plane but with a value close to zero. These exceptions reflect oscillations of the magnetic anisotropy for the smallest cluster sizes. More interestingly for Co/Ag(111) we also find a strong (10.98 meV/atom) out-of-plane anisotropy for the single atom case, which is highly sensitive to a lateral coordination with other cobalt atoms: a sudden easy-axis reorientation to the in-plane direction is predicted for the Co dimer case accompanied by an abrupt drop in the MAE absolute value (−1.23 meV/atom). After that, adding more atoms leaves the easy-axis direction in plane and the MAE varies only slightly with increasing number of atoms in the first layer, until reaching the ML value of −1.62 meV/atom. Stacking of Co atoms in a second layer reduces the absolute MAE value dramatically (almost a factor of 10) but does not change the easy-axis direction for islands with more than one atom. The positive MAE in the case of Co4 (three atoms in the first layer and one atom in the second) is due to the single Co atom in the second layer. A third layer of Co does not substantially change the situation anymore. Concerning the spin and orbital moments, we observe that they both decrease if the number of atoms in the island is increased, an effect known also from the literature.[19,23] The intra-atomic dipolar term decreases progressively in absolute value with increasing number of layers, indicating that the distribution of the magnetic moment is becoming more isotropic when the cluster is becoming more compact.

TABLE III. *Ab initio* calculations for the systems Co/Pt(111) and Co/Ag(111) calculated for ML height Co island with increasing number of atoms and for bilayer and trilayer height islands. In the table, average values for magnetic anisotropy (in millielectron volt per atom) and magnetic spin, orbital, and intra-atomic dipolar moment (in μ_B/atom) are reported. Positive (negative) values for the MAE indicate out-of-plane (in-plane) easy axes.

	MAE	μ_S	μ_L	μ_T
		ML cluster/Pt(111)		
Co1	4.88	2.269	0.604	−0.209
Co2	2.24	2.160	0.441	−0.045
Co3	−0.12	2.081	0.234	−0.088
Co7	−0.25	2.024	0.192	−0.025
Co19	0.22	1.967	0.168	
Co37	0.24	1.947	0.160	−0.047
		ML cluster/Ag(111)		
Co1	10.98	2.145	1.350	−0.023
Co2	−1.23	2.050	0.506	0.012
Co3	−2.71	2.009	0.410	0.012
Co7	−2.91	1.954	0.243	0.030
Co19	−1.60	1.915	0.221	−0.015
Co37	−1.78	1.899	0.214	−0.018
Monolayer	−1.62	1.872	0.186	−0.027
		Bilayer cluster/Ag(111)		
Co4	0.70	2.022	0.571	0.005
Co10	−0.235	1.921	0.277	0.016
Co31	−0.34	1.895	0.217	−0.006
Co64	−0.234	1.884	0.209	−0.007
		Trilayer cluster/Ag(111)		
Co39	−0.42	1.899	0.221	0.003
Co82	−0.21	1.888	0.210	0.0002

V. DISCUSSION

A. Growth dynamics of Co nanostructures on xenon buffer layers

Key observations during our study of the growth of Co on thick and thin Xe layers from the presented VT-STM experiments are (i) the observation of delayed Xe desorption in the vicinity of the Co clusters, (ii) differences in the cluster-substrate interaction for Ag and Pt substrates, resulting in a considerably stronger tendency for clusters to penetrate the Xe matrix for the case of Pt substrates, (iii) differences in the cluster morphology on Ag and Pt substrates, as well as cluster ripening during annealing of the samples to room temperature. In this paragraph we will discuss the processes of Xe desorption and cluster formation in more detail.

One of the most widely used concepts for thin film and cluster growth is the consideration of surface or interface energies of substrates and adlayers.[24] The interfacial energy γ^0_{AB} at the interface of two materials A and B is commonly expressed as $\gamma^0_{AB}=\gamma^0_A+\gamma^0_B+\Delta\gamma^{ads}_{AB}$, where γ^0_i is the surface free energy of material i and $\Delta\gamma^{ads}_{AB}$ the interfacial adhesion of the system AB. The $\Delta\gamma^{ads}_{AB}$ can be calculated (at zero temperature) for metal/Xe and metal/metal systems, using values for the surface free energy and interfacial adhesion from Ref. 24. We obtain interfacial energies γ^0_{AB} of 2.330 J/m^2,

0.230 J/m^2, and 0.007 J/m^2 for Co/Xe, Co/Ag, and Co/Pt, respectively. The gain in free energy upon formation of an interface between two materials can be written as: $\Delta\gamma=\gamma_A^0+\gamma_{AB}^0-\gamma_B^0$. Negative or very small values of $\Delta\gamma$ indicate that the formation of the interface is favored energetically and therefore a layer by layer growth is expected. In our case, for A=Co we found the values 1.530 J/m^2 and 0.007 J/m^2 for the two substrates B=Ag and Pt, respectively, that is Co wets Pt(111) but not Ag(111). Concerning the Xe/Co interface, one finds $\Delta\gamma=-0.188$ J/m^2 for Xe wetting the Co surface (A=Xe and B=Co). As already discussed in Ref. 25 for the case of Au nanoparticles on Xe, these results suggest that the Xe will coat the Co nanoparticles in order to minimize the surface energy.

Similar energy considerations can also be used to predict the morphology of the clusters in equilibrium. The Young-Dupré formula for a liquid droplet on a solid relates the contact angle θ of a droplet to the surface free energies of the solid and liquid, and the interfacial energy of the solid-liquid system: $\gamma_S^0=\gamma_{SL}^0+\gamma_L^0\cos\theta$. Special cases are complete wetting for $\theta=0°$ and a crossover from wetting to dewetting for $\theta=90°$. Evaluating the Co cluster morphology with this approach predicts total wetting for Co/Pt ($\theta=0°$), partial wetting for Co/Ag ($\theta=66.4°$), and dewetting for Co/Xe ($\theta=154°$). According to this estimate, the formation of a Co/metal substrate interface seems energetically most favorable, which could potentially destabilize the three-layer Co/Xe/metal system. Thus, the analysis of the surface free energies explains very well our experimental observation of the formation of hemispherical Co clusters on Xe/Ag and the differences of the cluster morphology after making contact with the Ag and Pt surface. Especially on the Pt(111) the strong tendency toward complete wetting results in the formation of monoatomically flat, epitaxial islands.

For a better understanding of the temperature-dependent dynamics during BLAG it is instructive to compare the desorption energies of Xe in different environments. The desorption energy for bulk Xe is 161 meV per xenon atom,[26] while for a single Xe monolayer on Ag(111) the desorption energy is 208 meV/atom,[27] and 286 meV/atom for 1 ML of Xe on Pt(111).[18] As already introduced in Sec. II A, the higher desorption energy for single Xe monolayers is due to interactions with the supporting substrate. Using the same argument, in the vicinity of surface step edges or clusters at the surfaces the Xe desorption can be delayed to even higher temperatures due to a higher coordination with the metal atoms, as seen in the STM images of Secs. II A and III A. A similar pinning effect has been reported for Ag clusters, soft landed on a Kr buffer layer.[28]

A difference in desorption energy between bulk Xe and a Xe monolayer adsorbed on a metal is expected to influence the growth mode of Co when directly deposited on Xe. The morphology of the two samples made with Ag(111) substrates and different Xe coverages suggests that Co coating by Xe atoms occurs on the bulk Xe, where the Xe desorption energy is lower. On the Xe single layer on Ag(111) instead Co atoms seem to simply diffuse on the Xe layer but with a higher diffusion coefficient compared to, e.g., a metal surface. A very special case is the Xe single layer on Pt(111), where the desorption energy is higher then on Ag(111) but the deposition of Co destroys the ML structure.

As a matter of fact, the required heat of desorption for a single Xe monolayer is determined by intralayer Xe-Xe interactions as well as Xe-substrate interactions. There are two different contributions to the Xe-Xe intralayer interactions, which are attractive van der Waals interaction and a repulsive contribution originating in the interaction between Xe and the substrate. The total lateral binding energy for 1 ML Xe/Ag(111) was reported to be 54.37 meV/atom.[27] Strain effects or the formation of induced dipoles in the Xe layer, for instance, can in fact increase the described repulsive contribution, hence weakening the total Xe-Xe interaction. The measured surface dipoles for Xe/Ag(111) is 0.2 D,[29] which corresponds to an average repulsive contribution of about 7 meV/Xe atom. For Xe/Pt(111), the induced dipole moment in the Xe layer is considerably higher, namely, 0.53 D, corresponding to an increased repulsive energy per Xe atom of 19 meV.[30] The higher surface dipole, together with other effects such as a higher work function, an unfilled d band, and stronger corrugation of the Pt(111) surface potential, contributes to a total lateral binding energy per Xe atom which is reduced by 30 meV/atom, compared to Ag(111).[17,31]

We argue here that the observation of Co cluster embedding in the Xe layer is a result of the described weakened Xe-Xe bonds and the presence of attractive van der Waals interaction between the Co and the metal substrate across the Xe buffer layer. For otherwise identical geometry the strength of the van der Waals interaction also depends on the dielectric function of the materials.[32] The presented comparison of BLAG on Pt and Ag substrates thus shows that the substrate can have a significant influence on the final size and shape of the clusters, as it determines the bond strength in a thin buffer layer, cluster-substrate interactions as well as the wetting behavior. As a result of the differences in BLAG, Co clusters on Pt(111) tend to be smaller and of flat shape, in comparison to Ag(111) substrates where the same BLAG parameters result in larger clusters of hemispherical shape. The above discussion is summarized in the growth model displayed in Fig. 5.

B. Analysis of the magnetic properties during Co self-assembly—Comparison to *ab initio* theory

In this section the measured magnetization as well as evaluated orbital and effective spin moments of the Co nanostructures during the different steps of BLAG (Tables I and II) are discussed in more detail since they allow for a correlation with the morphology information extracted from STM. Table IV shows an overview of magnetic moments in relevant geometries calculated with *ab initio* theory together with the values obtained from the XMCD sum rules.

First qualitative trends can be seen in the XMCD/XAS values at magnetic fields B=4.5 T given in Tables I and II. It is a well-known effect that spin and orbital moments are reduced as 3d clusters grow in size. Indeed, the XMCD/XAS values reflecting the average magnetization M is always smaller after Xe desorption, when the cluster size N is increased. When comparing M before Xe desorption then among the three measured samples cobalt on 12 ML of Xe

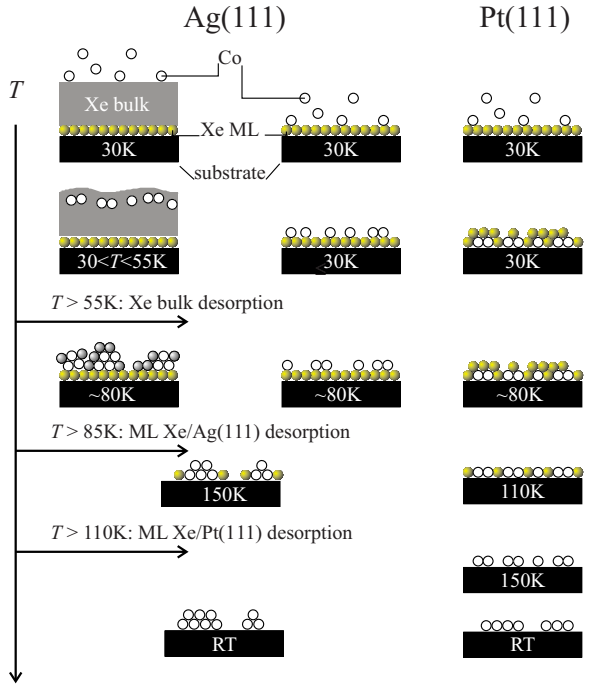

FIG. 5. (Color online) Detailed scheme of the cluster formation dynamics for the three different systems: Co/Xe buffer layer/Ag(111)(left), Co/Xe single layer/Ag(111)(center), and Co/Xe single layer/Pt(111)(right). The arrow on the left indicates the raising temperature T from top to bottom.

possesses the highest XMCD/XAS value of ≈0.7 in average but shows no magnetic anisotropy. This is coherent with the picture that smallest clusters on a thick Xe layer are electronically decoupled from the substrate. The same amount of Co on only 3.5 ML of Xe on Ag(111) shows already a slightly lower XMCD/XAS value of ≈0.6 in average but still no MAE. Finally the sample with 3.5 ML Xe on Pt(111) shows a similar value of XMCD/XAS ≈0.6 in average but a rather strong MAE.

In the following we want to address separately the results of orbital moments which are related to magnetic anisotropy effects, and trends in the spin moments.

Magnetic anisotropy and orbital moments. For a better understanding we briefly recall that the MAE is directly related to anisotropies of the orbital moments via the spin-orbit coupling constant ζ. In a simple case of a surface supported semispherical Co cluster a uniaxial MAE $\propto\zeta(\mu_L^{\parallel}-\mu_L^{\perp})$ is expected, assuming majority Co d bands are filled.[33] Here, $(\mu_L^{\parallel}-\mu_L^{\perp})$ is the anisotropy of the orbital moments parallel and perpendicular to the surface induced by the asymmetric environment of Co. In general a reduction in the Co orbital moments is related to the hybridization between Co d states with sp and d bands of the substrate and to internal d-d hybridization within the cluster. The latter of course increases with the average cluster size.

Comparing the two samples made with thick Xe layer and thin Xe layer on Ag(111) after annealing at 100 K. The values in Table IV indicate that the orbital moment of the former is smaller than the value found for the latter. This

TABLE IV. Average magnetic moments per atom in units μ_B for 0.05 ML Co on different substrates measured in the direction of the easy axis in a magnetic field of B=4.5 T. Expected values from theory for epitaxial monolayer and bilayer islands are shown in the lower part of the table. The number of holes in the d band was assumed to be n_h=2.49. Magnetic anisotropy energies are given in units of millielectron volt.

Experiment	μ_L/atom	$(\mu_S+7\mu_T)$/atom	Anisotropy/atom	Spin block size N	Size from STM
		Ag(111)-thick Xe layer			
Before annealing at 100 K (25 K)			Isotropic	35 ± 5	
After annealing at 100 K (8 K)	0.20 ± 0.10	1.14 ± 0.10			
After annealing at 100 K (35 K)	0.21	0.87	−0.15 ± 0.10	52	40 ± 7
		Ag(111)-thin Xe layer			
Before annealing at 100 K (25 K)	0.28	1.49	Isotropic	25	
After annealing at 100 K (8 K)	0.27	1.22	−0.10	18	
After annealing at 100 K (25 K)	0.27	0.93			16 ± 5
		Pt(111)-thin Xe layer			
Before annealing at 100 K (25 K)	0.39	1.35	0.59	17	
After annealing at 100 K (8 K)	0.29	1.43			
After annealing at 100 K (25 K)	0.25	1.20	0.67	18	6 ± 4
Theory	μ_L/atom	μ_S/atom	MAE/atom		
Co10/Ag(111) bilayer	0.277	1.921	−0.235	10	
Co31/Ag(111) bilayer	0.217	1.895	−0.34	31	
Co19/Pt(111) monolayer	0.168	1.967	0.22	19	
Co37/Pt(111) monolayer	0.160	1.947	0.24	37	
Co bulk[a]	0.154	1.62			

[a]Reference 12.

TABLE V. Overview of the experimental parameters used for the samples described in the text.

	STM		XMCD	
Substrate	Co (ML)	Xe (L)	Co (ML)	Xe (ML)
Ag(111)	0.05	50	0.05	12
Ag(111)	0.05	5	0.08	3–4
Pt(111)	0.05	5	0.06	3–4

decrease is possibly due to the internal *d-d* hybridization of the Co with increasing number of Co-Co neighbors in the cluster: the nanomagnets become larger, for higher Xe coverage. This is in agreement with the increase in spin block size N (see Table V), the STM investigation and the findings by Weaver *et al.*[2] We want to stress, however, that the error bar in the orbital moment evaluation is relatively large. Nevertheless, also the absolute values $\mu_L=0.27\mu_B$ per atom measured on Ag(111) are in good agreement with the calculations of bilayer islands of the experimentally derived cluster sizes $N=16$ (estimation from STM) and $N=18$ (spin block size): from Table III we expect μ_L to be $0.22-0.28\mu_B$. In Table III the quenching effect on μ_L with increasing cluster sizes is also shown by DFT-based calculations. Hybridization effects from the substrate are expected to be smaller for Ag(111) compared to Pt(111) since in the former case the full *d* band is shifted far below the Fermi level. Again this is reflected in the *ab initio* calculations, where for a given cluster geometry the orbital moments are higher for the case of Ag(111).

In the case of Pt(111) *ab initio* theory of monolayer islands with spin block sizes $N=25-30$ underestimates μ_L by about 30%. However, using the cluster size $N\approx 6$ estimated from STM leads to a much better agreement between experiment and theory. In the case of the Co/Xe/Pt(111) system we can compare our results to what was found by Gambardella *et al.*[34] for Co on Pt(111). A monolayer island of 7–8 atoms has a MAE of about 1 meV/atom and an orbital moment of about 0.35 μ_B/atom. Within the experimental errors, these numbers agree well with that of BLAG-grown Co clusters.

The well pronounced polar MAE observed already right after Co deposition on the Xe layer as compared to the lack of anisotropy for Co/Xe/Ag(111) indicates that in the first case the Co atoms and nanostructures cannot be considered as free. In our view the effect can only occur in presence of a broken symmetry as discussed in Ref. 34 that means a chemical bond with the Pt(111) surface. In line with what is discussed in Sec. V A on the STM results, we propose that Co penetrates the few Xe layers already at 25 K to make contact with the substrate.

Spin moments. The theoretical values of μ_S in Table III show that depending on the substrate the spin moment is expected to decrease monotonously by up to 14% when going from Co_1 to Co_{31} monolayer islands. In agreement with this trend, the experimentally determined effective spin moments $(\mu_S+7\mu_T)$ in Table IV are larger for the samples made with a thin buffer layer, where clusters are expected to be smaller. However, absolute experimental spin moments μ_S (the contribution of the intra-atomic magnetic dipole moment μ_T was accounted for using theory values in Table III) are smaller then those calculated for small clusters. For example, in the case of Co islands on Pt(111) we find spin moments of only $\mu_S=1.76$ μ_B/atom compared to the values $\mu_S=1.96$ μ_B/atom predicted by the calculations. The experimental value is thus more comparable to bulk values of 1.62 μ_B/atom,[12] where the spin moment is known to be reduced due to the large degree of Co-Co coordination. For the samples made on Ag(111) we even find Co spin moments which are below the bulk value. When comparing the Co/thin Xe layer/Ag(111) sample before and after bulk Xe desorption it is concluded that in the case of Ag(111) the reduction in the spin moment gets stronger with Xe desorption. The calculated spin values for ML cluster geometries in Table III support the more pronounced quenching effect for Ag(111) substrates although the magnitude is underestimated. In the following we discuss possible reasons for the small values of average spin moments in Co clusters.

(1) The geometry of the clusters formed under quasifree conditions on an inert Xe layer might play a role. In Ref. 35, for example, it was found that fcc mass selected free clusters, deposited on Au(111), have a spin moment of only about 1.5 μ_B/atom per atom, smaller than Co bulk, and smaller than what is found for epitaxial Co islands on Au(111) with a similar size.[36] Therefore it will be revealing to determine the crystalline structure of clusters made by BLAG. Experiments with this aim are currently in progress.

(2) Even though Co and Ag are immiscible, different scenarios might appear for deposition of minute amounts on surfaces.[37] Co-Ag intermixing could lead to the formation of a magnetically dead layer at the interface between clusters and Ag(111) with consequent reduction in the Co magnetic moment. This has been observed, for example, for Co/Ag multilayers,[38] where the Co moment of a 1-nm-thick Co layer was found to be quite small (about 1 μ_B/atom). Furthermore, according to calculations in Ref. 39 the spin moment of Co-Ag alloys could be reduced compared to the Co hcp bulk value, depending on the geometry and composition of the alloy, down to a value of about 1.3 μ_B/atom.

(3) A quenching of the spin moment of Co in contact with a nonmagnetic metal has been found for Co nanoclusters embedded in a Cu matrix.[40,41] The authors could attribute it to the cluster-matrix hybridization and presence of Rudermann-Kittel-Kasuya-Yosida (RKKY)-type cluster-cluster interactions. In our case, however, we exclude this explanation for two reasons. First, the average distances between clusters are larger then 2 nm which makes the RKKY intercluster interaction negligible. To give an order of magnitude, for Co_{32} clusters embedded in a Cu matrix[42] and cluster-cluster distances between 2 nm and 3 nm, calculated RKKY oscillations give interaction energies between 0.03 meV and 0.005 meV, respectively. At experimental temperatures of 8 K (0.7 meV) used in our experiments these interactions should not play a role. The second argument is the trend of magnetization versus cluster size and density: the magnetization is smaller for the sample made with 50 L Xe, which corresponds to larger clusters with smaller cluster density. Instead in Ref. 41 it was found that, as a consequence of

cluster-cluster interactions, the magnetization increases with the cluster size and, for a given size, decreases with the cluster concentration.

(4) Screening effects due to polarization of the Ag atoms surrounding the Co cluster is another possible explanation of the reduced spin moments. Recently, in an experiment on Co nanoparticles embedded in a Ag matrix,[43] Ag atoms were shown to exhibit a nonvanishing dichroic signal in an external magnetic field of 1 T. Although the induced Ag moments in the presence of Co atoms point in the same direction as those of Co, charge-transfer processes between Co and Ag need to be taken into account, which leads to incomplete filling of the Ag *d* bands and can decrease the average Co moments.

(5) Finally we want to consider the possibility of a noncollinear alignment of the Co atoms inside the cluster due to the interaction with the substrate, which can lead to a reduction in the average spin moments. One of the reasons for noncollinear magnetism is the Dzyaloshinskii-Moriya (DM) term, also called "anisotropic exchange interaction." This term is usually only important in the case of weak exchange interactions between magnetic atoms, which is why it is often not taken into account in most ferromagnetic systems. Contrary to that, recently it was calculated that in presence of a substrate with strong spin-orbit coupling[44] a noncollinear spin structure could be stabilized even in presence of strong ferromagnetic exchange interaction among atoms as in the case of a Co dimer. In particular, the authors suggest that DM couplings can affect the spin structure around the edges of larger nanostructures like those studied in this work.

VI. CONCLUSIONS

We have presented STM images and magnetic measurements on Co nanoclusters during different stages of Xe buffer-layer assisted growth. We find that Co clusters make direct contact with the Ag(111) only upon Xe desorption. On the contrary, on Pt(111) substrates Co clusters have a strong tendency to penetrate Xe layers of a few monolayer thickness until they get in contact with the substrate. We explain this behavior in terms of a complex interplay of Xe-Xe and Xe-substrate interactions. Electronic decoupling of the clusters and the substrate by a Xe buffer layer is therefore only achieved on Ag(111) substrates, leading to an absence of magnetic anisotropy in this case. The magnetic anisotropy of clusters in contact with Ag and Pt substrates is determined by the magnetic interface anisotropy and remanent out-of-plane magnetization is found for Co/Pt(111) at temperatures below 25 K. Cluster size effects and the contact with the substrate are also reflected in the spin and orbital magnetic moments. Trends obtained by XMCD could be reproduced in *ab initio* DFT calculations. From the calculations it is evident that magnetic properties like the orbital moments but especially the appearance of magnetic anisotropy is largely determined by cluster-substrate interface effects.

ACKNOWLEDGMENTS

We thank Júlio Criginski Cezar for the useful discussions. We acknowledge financial support from the DFG Schwerpunktprogramm SPP 1153.

APPENDIX: EXPERIMENTAL

VT-STM experiments were performed at the Max-Planck Institute for Solid State Research in Stuttgart, and XMCD experiments for magnetic characterization were done at the European Synchrotron Radiation Facility (ESRF) in Grenoble, beamline ID08. In both cases the samples were prepared and measured in UHV chambers with base pressure about 3×10^{-10} mbar. A precise determination of temperature, xenon and cobalt coverage as shown below ensured the comparability of the experiments.

The cobalt coverage was calibrated by a microbalance in the STM measurements and by the Co edge jump at the L_3 edge for the samples used in XMCD measurements. The xenon coverage was calibrated from the partial pressure in the UHV chamber (converted to Langmuir and then to film thicknesses in units of Ångströms) for the STM measurements and based on the saturation of the total electron yield (TEY) current upon xenon adsorption for the XMCD measurements (as described in more details in Ref. 45). The experimental parameters used to fabricate the samples described in the paper are displayed in Table V. The Ag(111) and Pt(111) substrates were cleaned by several sputtering/annealing cycles. Cleanliness and ordering of the crystal surface was verified by Auger, low-energy electron diffraction, and STM measurements. No contamination from oxygen and carbon monoxide were detected. During the XMCD measurements the oxygen contamination checks prior and after the measurements were done using XAS at the oxygen *K*-edge absorption line situated at 543.1 eV.

For all the experiments the xenon was preadsorbed on the sample at a temperature of about 30 K. At the same temperature Co was deposited from an e-beam evaporator. For the morphologic characterization, the sample was prepared in the manipulator and then transferred to the VT-STM that was precooled by liquid-helium flow. For magnetic characterization, the clean crystals were transferred to the magnet chamber under UHV conditions with a pressure of 1×10^{-10} mbar. In this case, adsorption of Xe and Co deposition were performed inside the high-field magnet chamber at ID08.

The XAS intensity was measured recording the total photoelectron yield as a function of the x-ray energy for positive (σ^+) and negative (σ^-) x-ray circular polarization ($99\pm1\%$ degree of polarization). Magnetic fields up to $B=4.5$ T were applied parallel and antiparallel to the photon beam. The angle of incidence of the beam was varied between $\phi=0°$ (normal incidence) and $\phi=70°$ (grazing incidence) to probe the out-of-plane and in-plane XMCD. The XAS signal is taken as the average intensity $(\sigma^+ + \sigma^-)/2$ and to the XMCD as $(\sigma^+ - \sigma^-)$. Hysteresis curves were measured recording the XMCD/XAS at the L_3 edge of cobalt as a function of magnetic field. The experimental time scales for measuring

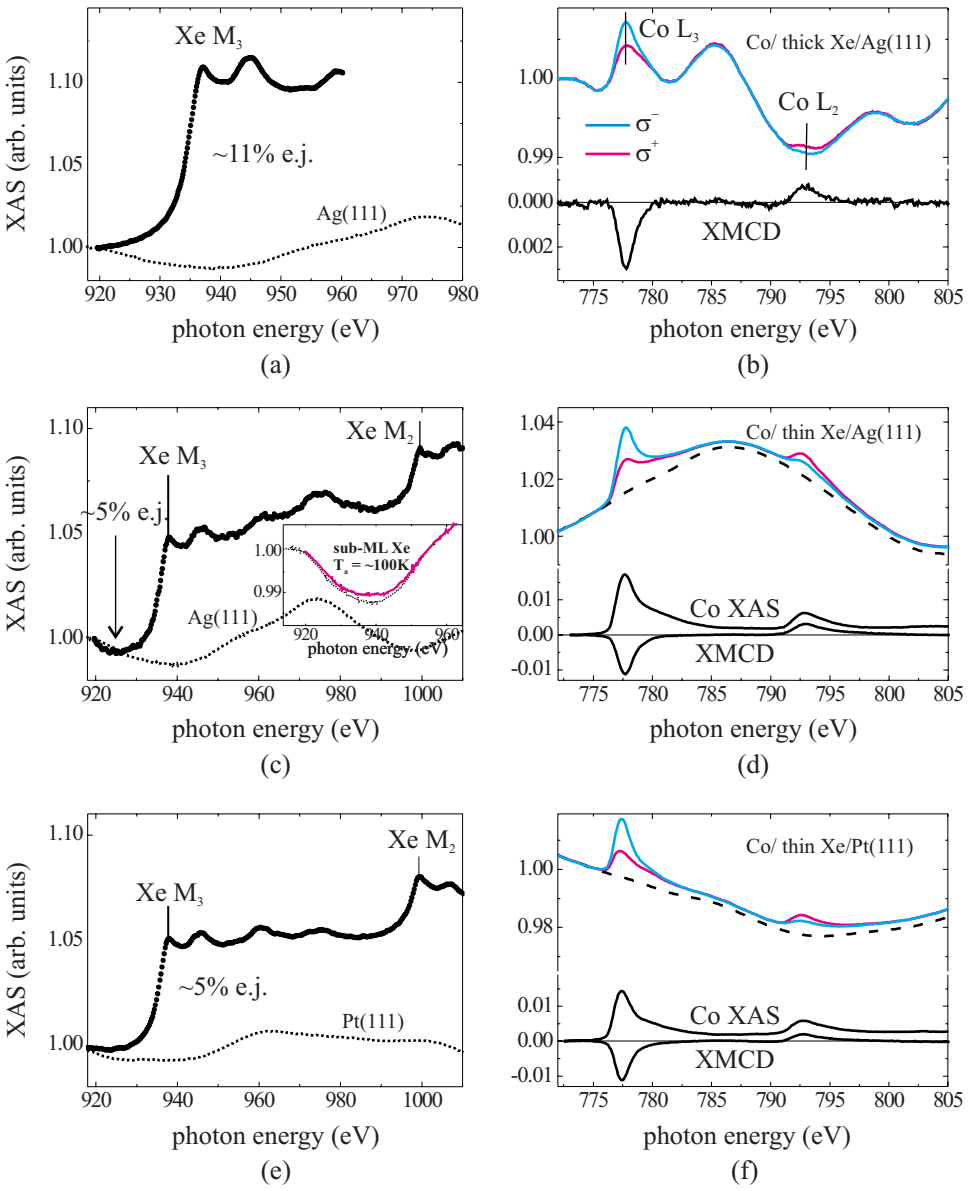

FIG. 6. (Color online) XAS signal for the three samples described in the text, showing the sample composition and dichroism right after deposition of Xe and Co at 25 K: Xe $M_{3,2}$ edges for (a) 12 ML Xe/Ag(111), (c) 3–4 ML Xe/Ag(111), and (e) 3–4 ML Xe/Pt(111); the substrate backgrounds (dotted line) are also plotted; Co $L_{3,2}$ edges for (b) 0.05 ML Co/12 ML Xe/Ag(111), (d) 0.08 ML Co/3–4 ML Xe/Ag(111), and (f) 0.06 ML Co/3–4 ML Xe/Pt(111); dashed lines indicate the Xe/substrate system backgrounds. The inset in (c) shows the XAS taken after annealing at 100 K for Xe/Ag(111) (pink colored line): a small amount of Xe (submonolayer coverage) is still present at this temperature on the Ag(111) surface.

spectra as well as ramping of the magnets to their designated values are on the order of 10–100 s. During the experiments no changes in the xenon lines induced by the heat load of the x rays were detected.

In Figs. 6(a), 6(c), and 6(e) XAS spectra at the xenon $M_{3,2}$ energy range show the Xe edge jump for 12 and 3–4 layers of Xe adsorbed on Ag(111) and Pt(111). Before Co deposition, the XAS background was also recorded at the energy range of the Co $L_{3,2}$ edge for the systems of interest: Ag(111), Pt(111) as well as xenon/Ag(111) and xenon/Pt(111). In Figs. 6(b), 6(d), and 6(f) we have the total electron yield signal for the three samples recorded right after Co deposition on the Xe/substrate at $T=25$ K. In (d) and (f) the background spectrum before Co evaporation is shown as a dashed line, which was used to separate the Co XAS shown in the same graph below. Also shown is the XMCD signal of cobalt indicating a sizable magnetic moment. In the last step of BLAG the sample was annealed at 100 K in order to desorb the Xe from the substrate being the nominal desorption temperature $T_{\mathrm{des}}^{\mathrm{substrate}}$ of the Xe monolayer from $T_{\mathrm{des}}^{\mathrm{Ag}} \approx 80$ K and $T_{\mathrm{des}}^{\mathrm{Pt}} \approx 110$ K. The measurements were repeated also after annealing the sample at 100 K. As we can see from the inset of Fig. 6, a submonolayer amount of Xe was still present on the Ag(111) substrate at these temperatures (pink colored line), due to the "pinning" of Xe atoms around the Co clusters. After annealing at 100 K it was verified that no oxygen contaminations appeared.

*Present address: European Synchrotron Radiation Facility, 6 rue Jules Horowitz, BP 220, 38043 Grenoble Cedex 9, France.
†Present address: School of Material Science and Engineering, Hebei University of Technology, Tianjin 300130, China.
‡j.honolka@fkf.mpg.de
§Present address: Diamond Light Source Ltd, Diamond House, Harwell Science and Innovation Campus, Didcot, Oxfordshire OX11 0DE, Great Britain.

[1] J. H. Weaver and G. D. Waddill, Science **251**, 1444 (1991).
[2] L. Huang, S. J. Chey, and J. H. Weaver, Phys. Rev. Lett. **80**, 4095 (1998).
[3] J. H. Weaver and V. N. Antonov, Surf. Sci. **557**, 1 (2004).
[4] T. R. Ohno, J. C. Patrin, U. S. Ayyala, and J. H. Weaver, Phys. Rev. B **44**, 1891 (1991).
[5] T. Irawan, D. Boecker, F. Ghaleh, C. Yin, B. von Issendorff, and H. Hövel, Appl. Phys. A **82**, 81 (2006).
[6] I. G. Marchenko and I. M. Neklyudov, Low Temp. Phys. **32**, 957 (2006).
[7] J. Zhang, D. Repetto, V. Sessi, J. Honolka, A. Enders, and K. Kern, Eur. Phys. J. D **45**, 515 (2007); and J. Zhang, V. Sessi, C. H. Michaelis, I. Brihuega, J. Honolka, K. Kern, R. Skomski, X. Chen, G. Rojas, and A. Enders, Phys. Rev. B **78**, 165430 (2008).
[8] J. Honolka, V. Sessi, S. Hertenberger, J. Zhang, A. Enders, and K. Kern, Phys. Status Solidi (to be published).
[9] C. Haley and J. H. Weaver, Surf. Sci. **518**, 243 (2002).
[10] L. W. Bruch, R. D. Diehl, and J. A. Venables, Rev. Mod. Phys. **79**, 1381 (2007).
[11] R. J. Behm, C. R. Brundle, and K. Wandelt, J. Chem. Phys. **85**, 1061 (1986).
[12] C. T. Chen, Y. U. Idzerda, H.-J. Lin, N. V. Smith, G. Meigs, E. Chaban, G. H. Ho, E. Pellegrin, and F. Sette, Phys. Rev. Lett. **75**, 152 (1995).
[13] P. Carra, B. T. Thole, M. Altarelli, and X. Wang, Phys. Rev. Lett. **70**, 694 (1993); B. T. Thole, P. Carra, F. Sette, and G. van der Laan, *ibid.* **68**, 1943 (1992).
[14] S. Bornemann, J. Minár, J. B. Staunton, J. Honolka, A. Enders, K. Kern, and H. Ebert, Eur. Phys. J. D **45**, 529 (2007).
[15] M. A. Chesters, M. Hussain, and J. Pritchard, Surf. Sci. **35**, 161 (1973).
[16] P. Dai, Z. Wu, T. Angot, S.-K. Wang, H. Taub, and S. N. Ehrlich, Phys. Rev. B **59**, 15464 (1999).
[17] K. Kern, R. David, P. Zeppenfeld, and G. Comsa, Surf. Sci. **195**, 353 (1988).
[18] W. Widdra, P. Trischberger, W. Frieß, D. Menzel, S. H. Payne, and H. J. Kreuzer, Phys. Rev. B **57**, 4111 (1998).
[19] O. Šipr, S. Bornemann, J. Minár, S. Polesya, V. Popescu, A. Šimůnek, and H. Ebert, J. Phys.: Condens. Matter **19**, 096203 (2007).
[20] S. H. Vosko, L. Wilk, and M. Nusair, Can. J. Phys. **58**, 1200 (1980).
[21] H. Ebert, Lect. Notes Phys. **535**, 191 (2000).
[22] J. Zabloudil, L. Szunyogh, P. Weinberger, and R. Hammerling, *Electron Scattering in Solid Matter* (Springer, New York, 2005).
[23] O. Šipr, J. Minár, and H. Ebert, Cent. Eur. J. Phys. **7**, 257 (2009).
[24] A. R. Miedema and B. E. Nieuwenhuys, Surf. Sci. **104**, 491 (1981).
[25] J. S. Palmer, P. Swaminathan, S. Babar, and J. H. Weaver, Phys. Rev. B **77**, 195422 (2008).
[26] C. W. Leming and G. L. Pollack, Phys. Rev. B **2**, 3323 (1970).
[27] S. Igarashi, A. Tosaka, T. Hirayama, and I. Arakawa, Langmuir **19**, 4627 (2003).
[28] R. Schaub, H. Jodicke, F. Brunet, R. Monot, J. Buttet, and W. Harbich, Phys. Rev. Lett. **86**, 3590 (2001).
[29] R. H. Roberts and J. Pritchard, Surf. Sci. **54**, 687 (1976).
[30] G. Schönhense, Appl. Phys. A: Solids Surf. **41**, 39 (1986).
[31] J. M. Gottlieb and L. W. Bruch, Phys. Rev. B **44**, 5759 (1991).
[32] J. N. Israelachvili, Proc. R. Soc. London, Ser. A **331**, 39 (1972).
[33] P. Bruno, Phys. Rev. B **39**, 865 (1989).
[34] P. Gambardella, S. Rusponi, M. Veronese, S. S. Dhesi, C. Grazioli, A. Dellmeyer, I. Cabria, R. Zeller, P. H. Dederichs, K. Kern, C. Carbone, and H. Brune, Science **300**, 1130 (2003).
[35] J. Bansmann, A. Kleibert, F. Bulut, M. Getzla, P. Imperia, C. Boeglin, and K.-H. Meiwes-Broer, Eur. Phys. J. D **45**, 521 (2007).
[36] T. Koide, H. Miyauchi, J. Okamoto, T. Shidara, A. Fujimori, H. Fukutani, K. Amemiya, H. Takeshita, S. Yuasa, T. Katayama, and Y. Suzuki, Phys. Rev. Lett. **87**, 257201 (2001).
[37] R. Q. Hwang, Phys. Rev. Lett. **76**, 4757 (1996).
[38] G. H. Yang, J. Chen, and F. Pan, Phys. Status Solidi A **194**, 71 (2002).
[39] L. T. Kong, R. F. Zhang, Z. C. Li, and B. X. Liu, Phys. Rev. B **68**, 134446 (2003).
[40] D. A. Eastham, Y. Qiang, T. H. Maddock, J. Kraft, J.-P. Schille, G. S. Thompson, and H. Haberland, J. Phys.: Condens. Matter **9**, L497 (1997).
[41] Y. Qiang, R. F. Sabiryanov, S. S. Jaswal, Y. Liu, H. Haberland, and D. J. Sellmyer, Phys. Rev. B **66**, 064404 (2002).
[42] D. Altbir, J. d'Albuquerque e Castro, and P. Vargas, Phys. Rev. B **54**, R6823 (1996).
[43] J. Bartolomé, L. M. García, F. Bartolomé, F. Luis, R. López-Ruiz, F. Petroff, C. Deranlot, F. Wilhelm, A. Rogalev, P. Bencok, N. B. Brookes, L. Ruiz, and J. M. González-Calbet, Phys. Rev. B **77**, 184420 (2008).
[44] S. Mankovsky, S. Bornemann, J. Minár, S. Polesya, H. Ebert, J. B. Staunton, and A. I. Lichtenstein, Phys. Rev. B **80**, 014422 (2009).
[45] V. Sessi, Ph.D. thesis, École Polytechnique Fédérale de Lausanne, 2010.